JACS
JOURNAL OF THE AMERICAN CHEMICAL SOCIETY

ARTICLE

pubs.acs.org/JACS

Evidence for Crystal-Face-Dependent TiO_2 Photocatalysis from Single-Molecule Imaging and Kinetic Analysis

Takashi Tachikawa,* Soichiro Yamashita, and Tetsuro Majima*

The Institute of Scientific and Industrial Research (SANKEN), Osaka University, Mihogaoka 8-1, Ibaraki, Osaka 567-0047, Japan

Supporting Information

ABSTRACT: According to the concept of active sites, the activity of heterogeneous catalysts correlates with the number of available catalytic sites and the binding affinity of the substrates. Herein, we report a single-molecule, single-particle fluorescence approach to elucidate the inherent photocatalytic activity of exposed surfaces of anatase TiO_2, a promising photocatalyst, using redox-responsive fluorogenic dyes. A single-molecule imaging and kinetic analysis of the fluorescence from the products shows that reaction sites for the effective reduction of the probe molecules are preferentially located on the {101} facets of the crystal rather than the {001} facets with a higher surface energy. This surprising discrepancy can be explained in terms of face-specific electron-trapping probability. In situ observation of the catalytic events occurring at the solid/solution interfaces reveals the hidden role of the crystal facets in chemical reactions and their impact on the efficiency and selectivity of heterogeneous (photo)catalysts.

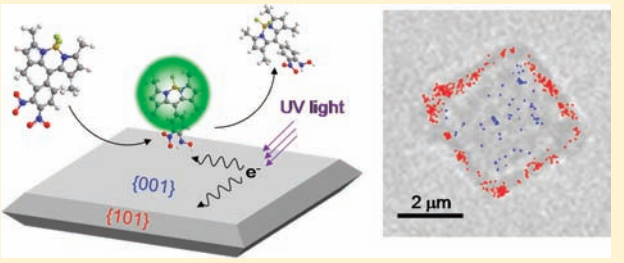

INTRODUCTION

In general, the catalytic activity of inorganic (nano)crystals is not only governed by their composition but also by the physicochemical properties of their exposed surfaces, which are related to their surface atomic arrangement and coordination.[1−3] Controlling the size, shape, and surface structures of the crystals at the nanoscale is a possible approach to improving the efficiency and selectivity of chemical reactions in heterogeneous catalysis.[4−6] Among the numerous varieties of metal oxides, anatase TiO_2 with either naturally or artificially defined {101} facets[7] is considered to be the most suitable photocatalyst material for energy and environmental sustainability.[8,9] Recently, Lu and co-workers reported a momentous step forward in the preparation of anatase TiO_2 single crystals with the highest energy surfaces.[10] They successfully synthesized high-quality anatase TiO_2 crystals with exposed {001} facets by using titanium fluoride (TiF_4) and hydrofluoric acid (HF) as the precursor and crystallographic controlling capping agent, respectively. Since then, significant efforts have been made to develop nano- and microsized TiO_2 crystals with a high percentage of specific facets; their superior performance in the photocatalytic degradation of organic compounds is regarded to be a benefit of the dominant {001} surfaces.[11−14] Despite these efforts, however, there remains an urgent need for a better understanding of the crystal face effects on TiO_2 photocatalysis, which could lead to breakthroughs in the rational design of novel materials for specific practical applications.

One of the principal difficulties in investigating this subject is the proper identification and resolution of the chemical reactions taking place on the heterogeneous surfaces under ambient conditions. To this end, single-molecule, single-particle spectroscopy (microscopy) is a very powerful tool for exploring the structural and kinetic features of "bulk" catalysis because of its high sensitivity and selectivity, simplicity of data collection, and high spatial and temporal resolution.[15−18] For example, Hofkens and co-workers studied the spatial distribution of catalytic activity on a layered double hydroxide using a wide-field microscope and a suitable fluorogenic probe to discover that ester hydrolysis proceeds on the lateral {1010} facets of the crystal, whereas transesterification occurs primarily on the {0001} planes.[19] We also recently applied the single-molecule, single-particle fluorescence imaging technique to identify the (photo)catalytically active sites on individual TiO_2 nanomaterials and their composites with noble metal nanoparticles[20−22] and to investigate the crystal-face dependence of interfacial electron transfer (ET) reactions on individual anatase TiO_2 crystals using a novel redox-responsive fluorogenic probe.[23] An important finding in this preliminary study[23] was that the energetically stable {101} facets of the crystal (the surface energy is 0.44 J m^{-2})[7] showed a higher photocatalytic reduction activity than the {001} facets with a higher surface energy (0.90 J m^{-2}). This observation is generally consistent with those previously obtained by the selective metal deposition method (e.g., platinum deposition).[24−26] However, the underlying fundamental issues, including face-specific molecular adsorption and charge transfer phenomena, have not been adequately investigated.

Herein, we provide definitive proof of the crystal-face dependency of the TiO_2 photocatalytic reactions along with detailed mechanisms. Single-molecule imaging and kinetic analyses of the fluorescence bursts emitted from the products reveal that the

Received: February 15, 2011
Published: April 15, 2011

dx.doi.org/10.1021/ja201415j | J. Am. Chem. Soc. 2011, 133, 7197–7204

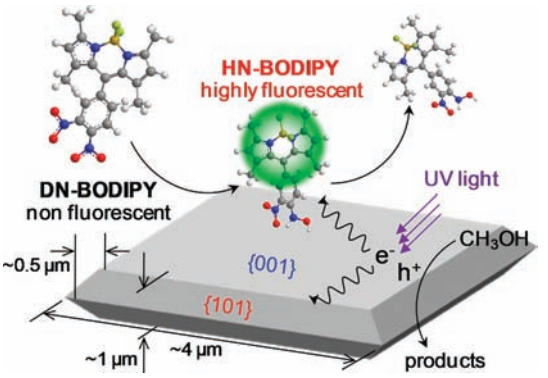

Figure 1. Photocatalytic generation of fluorescent HN-BODIPY from nonfluorescent DN-BODIPY over a TiO_2 crystal.

reaction selectivity on the {001} and {101} facets is primarily attributed to the crystallographic anisotropy in the trapping probability of the photogenerated charge carriers on the surfaces, which is presumably dependent on the number and distribution of potential trapping sites as well as their electronic energy levels.

RESULTS AND DISCUSSION

In Situ Observation of Photocatalytic Reductions Using a Fluorogenic Probe. The fluorogenic reaction is based on our recently developed ET-involved reduction of the boron-dipyrromethene compound 3,4-dinitrophenyl-BODIPY (DN-BODIPY; Figure 1).[22,23] Prior to reduction, the two nitro (NO_2) groups of the probe significantly decrease the lowest unoccupied molecular orbital (LUMO) energy level of the benzene moiety introduced at the meso position of the BODIPY core, thereby completely quenching the BODIPY fluorescence by an intramolecular ET from the excited fluorophore to the dinitrobenzene moiety. The reduction of one of the NO_2 groups to a hydroxylamino (NHOH) moiety results in an increase in the electron density, which is neutralized by the remaining NO_2 group, thereby dramatically suppressing the intramolecular ET process. Therefore, by accepting electrons, nonfluorescent DN-BODIPY ($\Phi_{fl} \approx 10^{-4}$ in methanol) can be reduced to form a highly fluorescent product, i.e., 4-hydroxyamino-3-nitrophenyl-BODIPY (HN-BODIPY, Φ_{fl} = 0.50 in methanol), which allows us to study the interfacial ET reaction on individual crystals via fluorescence detection of HN-BODIPY at the single-molecule level.

The photocatalytic activity of TiO_2 crystals was first evaluated using ensemble-averaged spectroscopy. The average size of the square sheetlike TiO_2 crystals is ca. 4 μm with a thickness of ca. 1 μm. When TiO_2 dispersions containing DN-BODIPY (50 μM, in Ar-saturated methanol) were exposed to 365 nm UV light, a new fluorescence peak appeared at ca. 510 nm; its intensity increased remarkably with increasing UV irradiation time (Figure S1, Supporting Information). In control experiments, the increase in fluorescence intensity was negligible when no TiO_2 photocatalyst was present in the solution. Because the photogenerated valence band holes (h^+) in TiO_2 are efficiently scavenged by methanol,[23,27] the photogenerated conduction band electrons (e^-) in TiO_2 are primarily responsible for the reduction of DN-BODIPY to generate the fluorescent product. A similar reaction pathway was reported for anatase TiO_2 nanocrystals (Ishihara Sangyo, A-100; the particle size is 100–200 nm), in which TiO_2 nanocrystals showed much higher photocatalytic reduction ability than microsized TiO_2 crystals used in this study.[22,23]

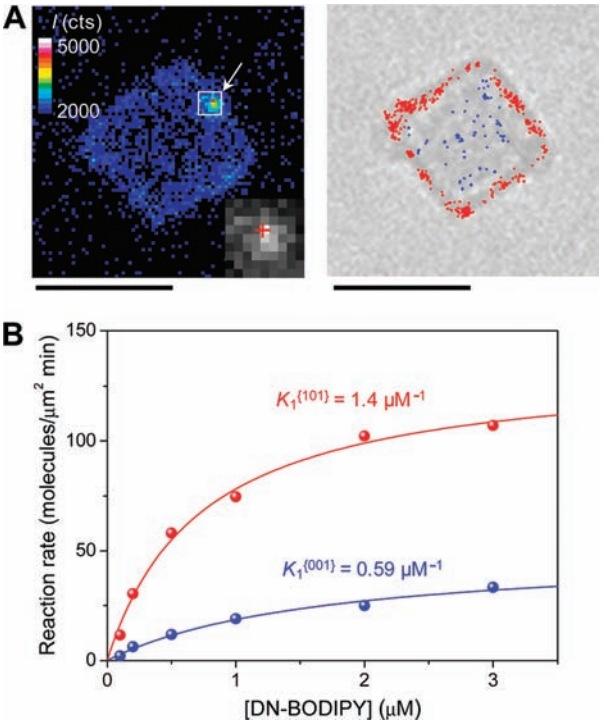

Figure 2. (A) Fluorescence (left) and transmission (right) images of the same TiO_2 crystal immobilized on a cover glass in Ar-saturated methanol solution containing DN-BODIPY (2.0 μM) under a 488 nm laser and UV irradiation. The scale bars are 4 μm. The inset of panel on the left shows the expanded image, as indicated by the arrow. The cross-mark shows the location of the reactive site. The blue and red dots in the transmission image indicate the location of fluorescence bursts on the {001} and {101} facets of the crystal, respectively, observed during 3 min irradiation. Images are adapted from ref 23. (B) DN-BODIPY concentration dependence of the reduction reaction rates obtained for {001} (blue) and {101} (red) facets of a single TiO_2 crystal (crystal 1, see Table 1). The solid lines were obtained from eq 1, and the fitting parameters for all crystals analyzed are summarized in Table 1.

Single-Molecule, Single-Particle Fluorescence Imaging. Total internal reflection fluorescence (TIRF) microscopy (Figure S2, Supporting Information) was used to investigate the crystal-face-dependent photocatalytic reduction of DN-BODIPY on individual TiO_2 crystals. Figure 2A shows a typical TIRF image captured for a single TiO_2 crystal in Ar-saturated methanol containing DN-BODIPY under a 488 nm laser and UV irradiation. A number of fluorescence bursts with signals higher than the background were observed during photoirradiation, and their locations, as determined using centroid analysis,[28] are likely distributed over the entire surface of the crystal (see the dots in the optical transmission image of Figure 2A). Control experiments confirmed that TiO_2, DN-BODIPY, and UV excitation are all essential to the generation of fluorescence bursts. Interestingly, fluorescence spots were found to be preferentially located on the lateral {101} facets of the crystal under all of the employed experimental conditions (see Movie S1, Supporting Information). The reaction rates for the generation of the product molecules were estimated to be 25 and 102 molecules μm^{-2} min^{-1} at [DN-BODIPY] = 2 μM for the {001} and {101} facets, respectively (Figure 2B). This result highlights a significant effect

dx.doi.org/10.1021/ja201415j |J. Am. Chem. Soc. 2011, 133, 7197–7204

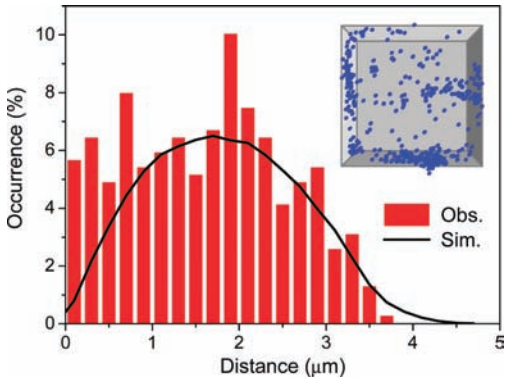

Figure 3. Histogram of reaction distance between successive two catalytic events. The black line indicates the simulation of distance between successive points (N = 100 000) randomly and uniformly distributed within the same domain (3.5 μm × 3.5 μm). The blue dots in the inset show the experimentally determined reactive sites.

of the crystal face on the photocatalytic activity, which is not evident in the bulk measurements. The repetition of the same experiments for inverted samples (i.e., an opposite {001} surface) under epi-illumination with a 488 nm laser provided essentially the same results (Figure S3, Supporting Information), thus confirming the accessibility of the probe molecules to the reactive sites on the crystal surface even under the TIRF configuration.

The spatial heterogeneity of the reactive sites was quantified by measuring the distance between the locations at which the fluorescence bursts were sequentially observed (Figure 3). In comparison to the spatial distribution for random points uniformly distributed within the restricted area (black curve) (see Figure S4 for calculations in the Supporting Information), the experimental data exhibit a reasonable fit in the whole distance range (red bars) but a noticeable difference below 500 nm owing to the clustering of catalytic events on either {101} or {001} or both. Furthermore, the structural characteristics of reactive sites were examined at the nanometer scale using a combination of single-molecule fluorescence localization microscope[29,30] and field emission scanning electron microscope (FE-SEM) analyses. A few objects with sizes of tens or hundreds of nanometers, which are most likely fragments of TiO_2 crystals or organic contaminants, were found on the surface; however, these objects have little or no role in the generation of fluorescence bursts (Figure S5A–D, Supporting Information). It is worthwhile to note here that surface cracks near the edges and corners are likely to serve as highly active sites (Figure S5E–H, Supporting Information). Therefore, crystals with a much larger heterogeneous distribution of reactive sites on the surface were excluded from further analysis to avoid contributions from the surface cracks (Figure S4, Supporting Information).

Fluorescence Lifetime Measurements. Fluorescence lifetime data measured using confocal microscopy with a time-correlated single-photon counting (TCSPC) system allowed us to ensure that the observed signals are from single dye molecules and also to gain further insight into the face-dependent interfacial ET dynamics, which directly influence the quantum efficiency of dye-sensitized solar cells and photocatalytic hydrogen generation.[31] As shown in Figure 4A, the fluorescence burst from the product, which is marked in red, can be easily distinguished from the background signal of DN-BODIPY in solution. The fluorescence

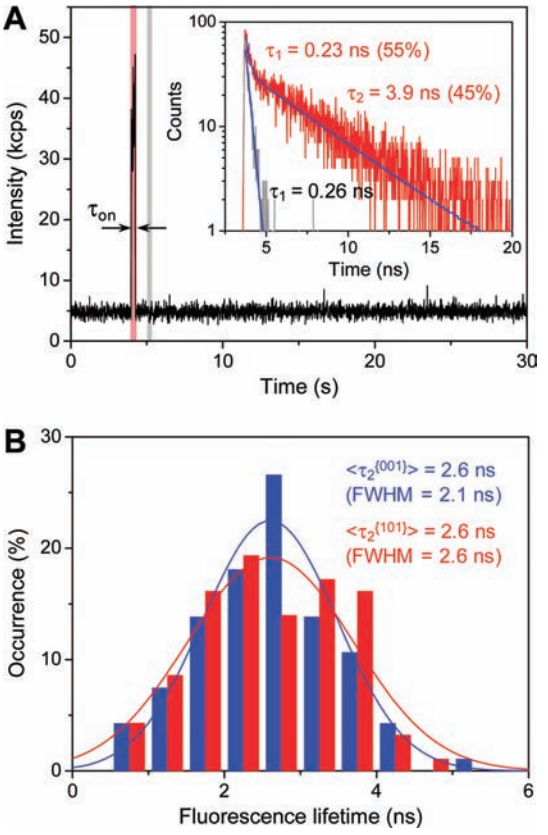

Figure 4. (A) Typical trajectory of fluorescence intensity observed for a single TiO_2 crystal in Ar-saturated DN-BODIPY solution (2.0 μM, methanol) under a 485 nm laser and UV irradiation. The inset shows the fluorescence decay profiles of the burst emission and background emission in the time regions indicated by red and gray in this panel, respectively. Blue lines indicate single- or double-exponential curves fitted to the data. The shorter and longer decay components are denoted as τ_1 and τ_2, respectively. (B) Histograms of fluorescence lifetimes (τ_2) of the bursts observed for the {001} (blue) and {101} (red) facets of five single TiO_2 crystals (over 93 events). The solid lines indicate the Gaussian distributions fitted with the histograms.

decay profiles were well-fitted by the biexponential function: $a_1 \exp(\tau/\tau_1) + a_2 \exp(\tau/\tau_2)$. The histograms of single-molecule fluorescence lifetimes (component 2) for the {001} and {101} facets of the crystal are described by a Gaussian distribution with a center of 2.6 ns and a full width at half-maximum (fwhm) of ~2–3 ns. These fluorescence lifetimes are shorter than those of free HN-BODIPY molecules in the bulk solution (τ = 3.7 ns) (Figure 4B), which implies the existence of interfacial ET from the excited BODIPY chromophore to TiO_2.[23,32] Moreover, the similar lifetime distributions for both surfaces indicate that there are no significant differences in the ET rate-determining parameters, such as the distance between the BODIPY chromophore and TiO_2, the reorganization energies of adsorbed dyes and surrounding solvent molecules, and the potential of the conduction band (vide infra).[33–38]

Crystal-Face Dependence of Adsorption Dynamics. Although the occurrences of the fluorescence bursts generated from one TiO_2 crystal are stochastic in nature, their statistical properties should provide valuable information regarding the kinetic mechanism of photocatalysis on TiO_2. As expected, the number of detected molecules is dependent on the concentration

dx.doi.org/10.1021/ja201415j |J. Am. Chem. Soc. 2011, 133, 7197–7204

Table 1. Kinetic Parameters Obtained for the {001} and {101} Facets of TiO_2 Crystals

	$k_{int}n_s$,[a] molecules μm^{-2} min^{-1}		K_1,[a] μM^{-1}		k_2,[b] s^{-1}		K_2,[b] μM^{-1}		k_3,[b] s^{-1}	
crystal no.	{001}	{101}	{001}	{101}	{001}	{101}	{001}	{101}	{001}	{101}
1	50 ± 5	135 ± 3	0.59 ± 0.13	1.4 ± 0.1	26 ± 2	7.5 ± 0.2	0.48 ± 1.3	3.5 ± 0.4	16 ± 1	16 ± 1
2	79 ± 4	314 ± 22	1.8 ± 0.3	1.9 ± 0.4	24 ± 3	7.0 ± 2.4	1.8 ± 2.2	2.2 ± 1.0	18 ± 3	36 ± 4
3	36 ± 2	257 ± 13	1.1 ± 0.2	0.34 ± 0.03	12 ± 4	1.3 ± 3	1.9 ± 2.2	0.50 ± 0.2	17 ± 4	18 ± 2
4	126 ± 7	175 ± 5	0.92 ± 0.13	0.64 ± 0.04	19 ± 2	4.4 ± 7.2	1.9 ± 0.8	1.3 ± 1.8	12 ± 2	24 ± 5
5	349 ± 27	225 ± 8	0.25 ± 0.03	0.64 ± 0.05	26 ± 8	5.7 ± 1.0	0.29 ± 0.21	2.7 ± 0.5	18 ± 2	16 ± 2
6	77 ± 2	260 ± 18	1.2 ± 0.1	0.53 ± 0.07	20 ± 1	4.4 ± 5.1	0.28 ± 0.04	0.17 ± 0.13	13 ± 1	13 ± 1
7	80 ± 10	269 ± 9	0.76 ± 0.18	1.3 ± 0.2	16 ± 2	3.6 ± 1.8	0.53 ± 0.15	1.1 ± 0.2	11 ± 1	19 ± 1
8	117 ± 11	152 ± 4	0.35 ± 0.04	0.76 ± 0.05	17 ± 7	9.4 ± 2.1	0.30 ± 0.6	0.85 ± 0.42	12 ± 2	18 ± 2
average	114 ± 35	223 ± 23	0.87 ± 0.18	0.93 ± 0.19	20 ± 2	5.4 ± 0.9	0.94 ± 0.27	1.5 ± 0.4	15 ± 1	20 ± 3

[a] Obtained from eq 1. [b] Obtained from eq 2.

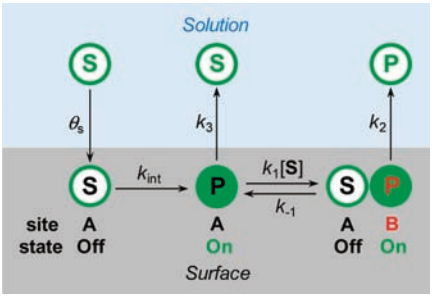

Figure 5. Schematic of the kinetic mechanism for photocatalytic reduction and product dissociation on TiO_2. **S** and **P** are the substrate (DN-BODIPY) and fluorescent product (HN-BODIPY), respectively. The sites **A** and **B** denote the original and alternative adsorption sites, respectively. k_{total} represents the combined reactivity of all surface catalytic sites ($=k_{int}n_s$). θ_s is the fraction of catalytic sites that are occupied by substrates ($=K_1[\mathbf{S}]/(1 + K_1[\mathbf{S}])$). When $[\mathbf{S}] \rightarrow 0$ or ∞, $\langle\tau_{on}\rangle^{-1}$ nearly equals k_3 or k_2, respectively (see eq 2).

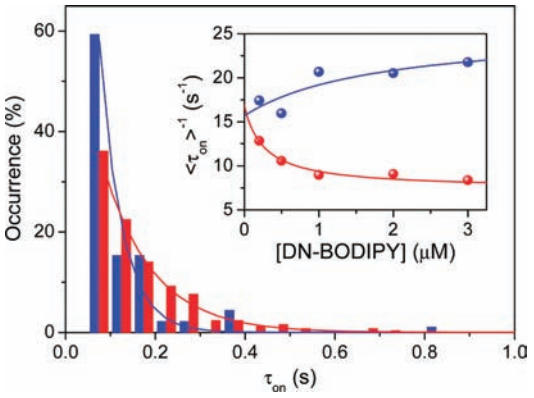

Figure 6. On-time distribution (τ_{on}) constructed from over 100 events for the {001} (blue) and {101} (red) facets of a single TiO_2 crystal, respectively. The solid lines indicate the Gaussian distributions fitted with the histograms. Inset shows the DN-BODIPY concentration dependence of $\langle\tau_{on}\rangle^{-1}$ obtained for the {001} (blue) and {101} (red) facets of a single TiO_2 crystal (crystal 1, see Table 1). The solid lines in the inset were obtained from eq 2, and the fitting parameters for all analyzed crystals are summarized in Table 1.

of DN-BODIPY (Figure 2B). At higher concentrations, the reaction rate of the reduction of DN-BODIPY to its fluorescent products is faster, leading to an increase in the number of HN-BODIPY molecules.

The substrate-concentration ([**S**]) dependence of the total product formation rate per crystal (k_{total}) can be described using the Langmuir−Hinshelwood equation:

$$k_{total} = \frac{k_{int}n_sK_1[\mathbf{S}]}{1 + K_1[\mathbf{S}]} \quad (1)$$

where K_1 is the equilibrium adsorption constant for the substrate, k_{int} is the intrinsic rate constant for one catalytic site, and n_s is the total number of substrate binding sites on the crystal.[39,40] There is a great deal of variation in these parameters from crystal (facet) to crystal (facet), reflecting the heterogeneous nature of photocatalysis (see Table 1). For example, the crystal depicted in Figure 2B provides K_1 values of 0.59 ± 0.13 and 1.4 ± 0.1 μM^{-1} for the adsorption of DN-BODIPY on the {001} and {101} facets, respectively. The average K_1 values over eight different crystals were calculated to be 0.87 ± 0.18 and 0.93 ± 0.19 μM^{-1} for the {001} and {101} facets, respectively, which are of the same order of magnitude as those for nitrobenzenes.[41] On average, the adsorptivity of DN-BODIPY on the *original* adsorption site (i.e., site **A** in Figure 5) is almost equivalent for both TiO_2 surfaces.

To follow the dissociation pathway of individual product molecules from the surface into the bulk solution, a statistical analysis of the characteristic time τ_{on} during which persistent emission is exhibited (e.g., see Figure 4A) was conducted. As depicted in Figure 6, the distributions of τ_{on} fit well with a single-exponential decay function ($R^2 > 0.97$), and the inverses of the average values of τ_{on} ($\langle\tau_{on}\rangle$) determined were plotted against [**S**] (inset of Figure 6). Interestingly, an opposite concentration dependence of $\langle\tau_{on}\rangle^{-1}$ was observed for the {001} and {101} facets of the crystal. Our previous experiments showed that photobleaching or blinking of single HN-BODIPY molecules occurs on much longer time scales than $\langle\tau_{on}\rangle$ under similar laser intensities, thus suggesting that the observed sudden decreases in intensity are mainly due to the dissociation of HN-BODIPY.[22,23]

According to the literature,[39,40] the main feature of the kinetics of "substrate-assisted" product dissociation is described as

$$\langle\tau_{on}\rangle^{-1} = \frac{k_2K_2[\mathbf{S}] + k_3}{1 + K_2[\mathbf{S}]} \quad (2)$$

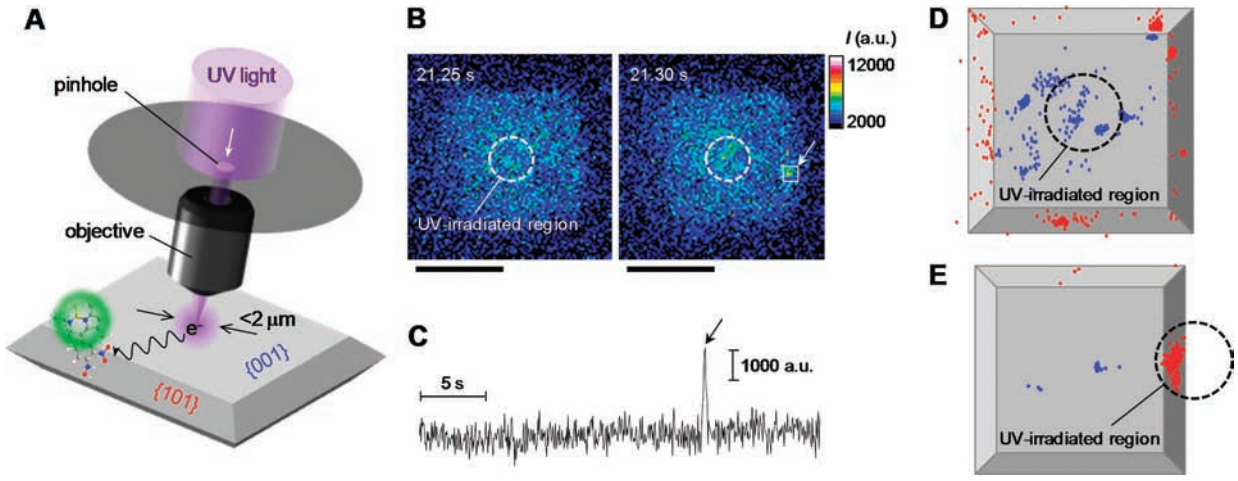

Figure 7. (A) Illustration of the remote photocatalytic reaction on the {101} facets with DN-BODIPY during photoirradiation onto the {001} facets. The irradiated area was limited by a pinhole (the spot diameter is 2 μm on the crystal surface). (B) Fluorescence image of a TiO_2 crystal that is immobilized on the cover glass in Ar-saturated DN-BODIPY solution (1.0 μM, in methanol) under a 488 nm laser and UV irradiation. The scale bars are 4 μm. (C) Time trace of fluorescence intensity observed over the square region in panel B (see the arrow). The UV irradiation area is inside the white circle in the images. (D, E) Location of fluorescence bursts on the {001} (blue) and {101} (red) facets. The UV irradiation areas are inside the black circles (diameter 2 μm).

where k_2 is the rate constant of product dissociation in the substrate-assisted pathway, k_3 is the rate constant of direct product dissociation, and $K_2 = k_1/(k_{-1} + k_2)$. By fitting eq 2 to the experimental data, all of the rate and equilibrium constants were determined, as given in Table 1.

The initial step in all the catalytic reaction pathways is the adsorption of substrates on the exposed atoms on the surface. The high surface energy of the {001} facets is likely a consequence of the high density of surface undercoordinated Ti atoms (e.g., 7.0×10^{-2} and 5.1×10^{-2} Å^{-2} for 5-fold Ti atoms on the (001) and (101) surfaces, respectively).[7] Nonetheless, the averaged values of both K_1 and k_3 are essentially the same between the {101} and {001} facets, suggesting that the **A** sites on the two facets are the same. Because perfect {101} and {001} facets have different surface sites, one reasonable interpretation is that the **A** sites are defect sites, such as oxygen vacancies.[9,42,43] If the catalytic reactivities on both facets are dominated by the defect sites, rather than surface structures determined by the facets, the difference between $k_{int}n_s$ of the two facets should be simply due to the difference in n_s, not in k_{int}.

A striking difference is found in the dissociation dynamics of HN-BODIPY from the *alternative* binding site (i.e., site **B** in Figure 5), where the product is readsorbed after being replaced by the substrate. The average k_2 value ((20 ± 2) s^{-1}) was close to the average k_3 value ((15 ± 1) s^{-1}) for the {001} facets, while the average k_2 value ((5.4 ± 0.9) s^{-1}) was much smaller than the average k_3 value ((20 ± 3) s^{-1}) for the {101} facets. These results strongly suggest that the removal of HN-BODIPY from the {101} facets involves substrate-assisted steps. Until now, molecular-level investigations of catalytic reactions have been performed on TiO_2 single-crystal surfaces using surface specific vibrational spectroscopy and scanning tunneling microscopy (STM). For example, sum frequency generation (SFG) and theoretical calculation studies showed that the higher density of 5-fold Ti atoms on the (001) facets leads to the dissociative adsorption of methanol.[44,45] Due to its higher binding energy, the dissociatively adsorbed methanol (i.e., Ti−OCH_3 species) as a coadsorbate would inhibit the readsorption of HN-BODIPY onto the {001} facets and quench the surface defects, which also act as trap sites for photogenerated electrons.[9,21] On the other hand, HN-BODIPY molecules produced on the {101} facets cause readsorption at a favorable site, because the methanol molecules are weakly adsorbed on the surface via hydrogen bonding.[44,45]

Anisotropic Electron Flow in TiO_2. The photogenerated electrons and holes in the bulk of TiO_2 migrate to the surface and then participate in redox processes at the surface or recombine with each other within a few nanoseconds.[27] The spatial separation of these charge carriers in individual catalyst particles is thus expected to reduce the recombination probability and simultaneously enhance the reaction efficiency and selectivity. To address this issue and examine the crystal-face dependence of the electron-trapping processes at the surfaces, we have performed further experiments.

As illustrated in Figure 7A, a center part of the {001} facet of the crystal was irradiated by UV light through a 100 μm pinhole (Figure S6, Supporting Information). Interestingly, a number of fluorescence bursts were still observed on the unirradiated {101} facets in addition to the {001} surface (Figure 7B−D). A similar tendency was observed for more than five individual crystals that were examined. In contrast, the catalytic activity on the {001} facet was much lower or negligible during the selective UV irradiation on the {101} facet (Figure 7E). These results imply that the {101} facets serve as possible reservoirs of the photogenerated electrons. In fact, density functional theory (DFT) calculations predicted that the conduction band potential of anatase (101) is slightly lower than that of anatase (001)[46] and, moreover, that the exposed (101) facet yields a highly reactive surface for the reduction of O_2 molecules to superoxide radicals.[47] Such a small difference in the conduction band edge does not actually influence the ET rates from the excited dye molecules to TiO_2, owing to the large density of accepting states (see Figure 4B), but would have a significant effect on the electron flow across the interfaces.

To prove our hypothesis, we measured the defect-mediated photoluminescence of individual TiO_2 crystals by 405 nm laser

dx.doi.org/10.1021/ja201415j |*J. Am. Chem. Soc.* 2011, 133, 7197–7204

excitation under an Ar atmosphere. The results are shown in Figure S7 (Supporting Information). A substantial increase in the emission intensity observed during photoirradiation is attributable to various defects associated with oxygen vacancies in the TiO_2 (so-called "color centers"),[48] as was already proven for other TiO_2 nanomaterials.[21,49] It should be noted that the {101} facets exhibited a higher emission intensity, compared to that of the {001} facets. Photoactivation of the TiO_2 crystals was also accompanied by a dramatic spectral change (Figure S7B,C). The component around 600 nm, which originates from surface-trapped electrons, increased more significantly than that around 525 nm.[21] This spectral feature is more clearly seen on the {101} facets of the crystal (panel C), thus supporting the preferential trapping of electrons at the surface and/or subsurface defects on these facets.[50] Consequently, the trapped electrons are efficiently transferred to DN-BODIPY on the {101} facets; this results in the increase of k_{int} (see eq 1).

A fundamental question still arises: what is the oxidation reactivity of the {001} and {101} facets? According to the literature,[24,26] it is likely that the {001} facets are a predominantly oxidative surface. The DFT calculations also indicated that the contribution of undercoordinated 2-fold O atoms on the (001) surface to the upper edge of valence band is responsible for its activity in methanol.[51] To obtain specific information about the crystal-face dependence in photocatalysis, we explored the oxidation reactivity of the {001} and {101} facets of individual TiO_2 crystals under UV irradiation using an oxidation-responsive fluorogenic probe: i.e., 4-aminophenyl-BODIPY (NH_2-BODIPY) (see the Supporting Information for details). As shown in Figure S8 (Supporting Information), the single-particle analysis convincingly demonstrates that the {001} facets yield a similar or slightly higher adsorption affinity and reactivity toward the aminophenyl moiety of the probe, compared to that of the {101} facets. This observation is in accordance with the results of the aforementioned investigations and emphasize a unique and important role of the {101} surfaces as the reductive site in TiO_2 photocatalysis.

CONCLUSIONS

As mentioned in the Introduction, the crystal facets with a higher surface energy are believed to offer highly reactive sites for heterogeneous (photo)catalysis. Providing the first evidence contrary to this prediction, we have shown the surface-energy-independent distribution of available reactive sites within one TiO_2 crystal using spatially and temporally resolved fluorescence measurements with single-molecule redox sensors. Careful and thorough examinations of the photocatalytic reactions on individual crystals could exclude the possible influence of the aggregation or precipitation of particles formed in the bulk solution, which probably masks the intrinsic reactivity of the crystal facets. Moreover, we have verified the hypothesis that the directional flow of photogenerated charge carriers toward specific surfaces improves the reaction efficiency and selectivity. Another important finding of this study is that molecular desorption kinetics are strongly associated with the surface structures of the exposed crystal facets. The interplay of molecular motion and transformation on catalyst surfaces, especially for aromatic compounds, is a current topic of interest.[52,53] Although the atomic-scale identification of the reactive sites remains a challenge, our single-molecule, single-particle approach provides valuable insight into the mechanism of TiO_2 photocatalytic reactions and will be applicable for reliable real-time detection of redox events in heterogeneous catalysis and, furthermore, in biological systems.

MATERIALS AND METHODS

Synthesis of Fluorogenic Probes. 8-(3,4-Dinitrophenyl)-1,3,5,7-tetramethyl-4,4-difluoro-4-bora-3a,4a-diaza-*s*-indacene (DN-BODIPY) was synthesized as previously reported.[23] 8-(4-Aminophenyl)-1,3,5,7-tetramethyl-4,4-difluoro-4-bora-3a,4a-diaza-*s*-indacene (NH_2-BODIPY) was synthesized according to the procedures reported in the literature with some modifications. The details of the procedures and characterizations are given in the Supporting Information.

Preparation of TiO_2 Crystals. Microsized anatase TiO_2 single crystals with dominant {001} facets were hydrothermally synthesized according to the procedure reported by Liu et al.[10,54] In a typical procedure, 30% titanium sulfate solution (Wako) was dissolved in 0.2 M hydrofluoric acid (HF) solution and the mixture was heated in a Teflon-lined stainless steel autoclave at 180 °C for 5.5 h. ***Caution!*** *Hydrofluoric acid (HF) is extremely corrosive and is a contact poison. It should be handled with extreme care.* The resulting material was separated by centrifugation for 10 min at 10 000 rpm, repeatedly washed with Milli-Q water until pH 7, and then dried overnight at 120 °C. To remove surface fluorine species, the powders were heated at 600 °C for 90 min before use. The results of structural characterizations of synthesized TiO_2 crystals were previously reported.[23]

Sample Preparation for Single-Molecule Fluorescence Experiments. To obtain isolated TiO_2 crystals, well-dispersed methanol suspensions at very low concentrations of TiO_2 were spin-coated on a cleaned cover glass. The particle-coated cover glass was annealed at 363 K for 30 min to immobilize the crystals on the glass surface, and then placed in a flow chamber (Chamlide, CF-T25). An Ar-saturated sample solution was then introduced into this chamber in an Ar-purged glovebox ($[O_2]$ < 0.5 vol %). Details of the sample preparation are given in the Supporting Information.

Single-Molecule Fluorescence Measurements by Wide Field Microscopy. The experimental setup was based on an Olympus IX71 inverted fluorescence microscope.[23] The position of the TiO_2 crystals immobilized on the cover glass was determined from the transmission image obtained by illuminating the samples using a halogen lamp (Olympus, U-LH100L-3). A circularly polarized light emitted from a CW Ar ion laser (Melles Griot, IMA101010BOS; 488 nm, 0.1 kW cm^{-2} at the glass surface) was reflected toward a second dichroic mirror (Olympus, DM505) using a first dichroic mirror (Olympus, RDM450), which reflected wavelengths longer than 450 nm and was transparent to wavelengths shorter than 450 nm. The laser light passing through an objective lens (Olympus, UPLSAPO 100XO; 1.40 NA, 100×) after reflection by a second dichroic mirror was completely reflected at the cover glass−methanol interface. This resulted in the generation of an evanescent field, which made it possible to detect a single fluorescence dye molecule. For excitation of the TiO_2 crystals, the 365 nm light, which was emitted by an LED (OPTO-LINE, MS-LED-365; 30 mW cm^{-2} at the glass surface) and passed through an ND filter, was passed through the objective. The fluorescence emission from the fluorescent products generated on a single TiO_2 crystal on the cover glass was collected using the same objective, after which it was magnified by a 1.6× built-in magnification changer, passed through a bandpass filter (Semrock, FF01-531/40-25) to remove the undesired scattered light, and then imaged using an electron-multiplying charge-coupled device (EM-CCD) camera (Roper Scientific, Cascade II:512). The images were recorded at a frame rate of 20 frames s^{-1} and processed using ImageJ (http://rsb.info.nih.gov/ij/) or OriginPro 8.1 (OriginLab). All experimental data were obtained at room temperature.

Single-Molecule Fluorescence Measurements by Confocal Microscopy. Confocal fluorescence images were recorded using an objective-scanning confocal microscope system (PicoQuant, MicroTime 200) coupled with an Olympus IX71 inverted fluorescence microscope. The samples were excited through an oil-immersion objective lens (Olympus, UAPON 150XOTIRF; 1.45 NA, 150×) using a 485 nm pulsed laser (PicoQuant, LDH-D-C-485; 2 kW cm^{-2} at the glass surface) controlled by a PDL-800B driver (PicoQuant). The emission from the sample was collected using the same objective and detected by a single photon avalanche photodiode (Micro Photon Devices, PDM 50CT) through a dichroic beam splitter and bandpass filter (Semrock, FF01-531/40-25). All experimental data were obtained at room temperature.

■ ASSOCIATED CONTENT

Supporting Information. Text and figures giving experimental details, including the descriptions of the experimental and analytical procedures, the preparation and characterization of materials, and additional results, and a movie showing the single-molecule fluorescence imaging of the reduction of DN-BODIPY on TiO_2 (Movie S1). This material is available free of charge via the Internet at http://pubs.acs.org.

■ AUTHOR INFORMATION

Corresponding Author
tachi45@sanken.osaka-u.ac.jp; majima@sanken.osaka-u.ac.jp

■ ACKNOWLEDGMENT

We thank to Ms. Nan Wang for preparation of fluorogenic probes. T.M. thanks the WCU (World Class University) program through the National Research Foundation of Korea funded by the Ministry of Education, Science and Technology (R31-10035) for support. This work has been partially supported by a Grant-in-Aid for Scientific Research (Projects 22245022, 21750145, and others) from the Ministry of Education, Culture, Sports, Science and Technology (MEXT) of the Japanese Government.

■ REFERENCES

(1) Taylor, H. S. *Proc. R. Soc. London, Ser. A* **1925**, *108*, 105–111.
(2) Zambelli, T.; Wintterlin, J.; Trost, J.; Ertl, G. *Science* **1996**, *273*, 1688–1690.
(3) Tao, F.; Salmeron, M. *Science* **2011**, *331*, 171–174.
(4) Yin, Y.; Alivisatos, A. P. *Nature* **2005**, *437*, 664–670.
(5) Burda, C.; Chen, X.; Narayanan, R.; El-Sayed, M. A. *Chem. Rev.* **2005**, *105*, 1025–1102.
(6) Somorjai, G. A.; Frei, H.; Park, J. Y. *J. Am. Chem. Soc.* **2009**, *131*, 16589–16605.
(7) Lazzeri, M.; Vittadini, A.; Selloni, A. *Phys. Rev. B: Condens. Matter Mater. Phys.* **2001**, *63*, 155409/155401–155409/155409.
(8) Fujishima, A.; Zhang, X.; Tryk, D. A. *Surf. Sci. Rep.* **2008**, *63*, 515–582.
(9) Thompson, T. L.; Yates, J. T., Jr. *Chem. Rev.* **2006**, *106*, 4428–4453.
(10) Yang, H. G.; Sun, C. H.; Qiao, S. Z.; Zou, J.; Liu, G.; Smith, S. C.; Cheng, H. M.; Lu, G. Q. *Nature* **2008**, *453*, 638–641.
(11) Wu, B.; Guo, C.; Zheng, N.; Xie, Z.; Stucky, G. D. *J. Am. Chem. Soc.* **2008**, *130*, 17563–17567.
(12) Yang, H. G.; Liu, G.; Qiao, S. Z.; Sun, C. H.; Jin, Y. G.; Smith, S. C.; Zou, J.; Cheng, H. M.; Lu, G. Q. *J. Am. Chem. Soc.* **2009**, *131*, 4078–4083.
(13) Han, X.; Kuang, Q.; Jin, M.; Xie, Z.; Zheng, L. *J. Am. Chem. Soc.* **2009**, *131*, 3152–3153.
(14) Amano, F.; Yasumoto, T.; Prieto-Mahaney, O.-O.; Uchida, S.; Shibayama, T.; Ohtani, B. *Chem. Commun.* **2009**, 2311–2313.
(15) Weckhuysen, B. M. *Angew. Chem., Int. Ed.* **2009**, *48*, 4910–4943.
(16) De Cremer, G.; Sels, B. F.; De Vos, D. E.; Hofkens, J.; Roeffaers, M. B. J. *Chem. Soc. Rev.* **2010**, *39*, 4703–4717.
(17) Chen, P.; Zhou, X.; Shen, H.; Andoy, N. M.; Choudhary, E.; Han, K.-S.; Liu, G.; Meng, W. *Chem. Soc. Rev.* **2010**, *39*, 4560–4570.
(18) Tachikawa, T.; Majima, T. *Chem. Soc. Rev.* **2010**, *39*, 4802–4819.
(19) Roeffaers, M. B. J.; Sels, B. F.; Uji-i, H.; De Schryver, F. C.; Jacobs, P. A.; De Vos, D. E.; Hofkens, J. *Nature* **2006**, *439*, 572–575.
(20) Naito, K.; Tachikawa, T.; Fujitsuka, M.; Majima, T. *J. Am. Chem. Soc.* **2009**, *131*, 934–936.
(21) Tachikawa, T.; Majima, T. *J. Am. Chem. Soc.* **2009**, *131*, 8485–8495.
(22) Wang, N.; Tachikawa, T.; Majima, T. *Chem. Sci.* **2011**, *2*, 891−900.
(23) Tachikawa, T.; Wang, N.; Yamashita, S.; Cui, S.-C.; Majima, T. *Angew. Chem., Int. Ed.* **2010**, *49*, 8593–8597.
(24) Ohno, T.; Sarukawa, K.; Matsumura, M. *New J. Chem.* **2002**, *26*, 1167–1170.
(25) Taguchi, T.; Saito, Y.; Sarukawa, K.; Ohno, T.; Matsumura, M. *New J. Chem.* **2003**, *27*, 1304–1306.
(26) Murakami, N.; Kurihara, Y.; Tsubota, T.; Ohno, T. *J. Phys. Chem. C* **2009**, *113*, 3062–3069.
(27) Tachikawa, T.; Fujitsuka, M.; Majima, T. *J. Phys. Chem. C* **2007**, *111*, 5259–5275.
(28) Sage, D.; Neumann Franck, R.; Hediger, F.; Gasser Susan, M.; Unser, M. *IEEE Trans. Image Process.* **2005**, *14*, 1372–1383.
(29) Roeffaers, M. B. J.; De Cremer, G.; Libeert, J.; Ameloot, R.; Dedecker, P.; Bons, A.-J.; Bueckins, M.; Martens, J. A.; Sels, B. F.; De Vos, D. E.; Hofkens, J. *Angew. Chem., Int. Ed.* **2009**, *48*, 9285–9289.
(30) De Cremer, G.; Roeffaers, M. B. J.; Bartholomeeusen, E.; Lin, K.; Dedecker, P.; Pescarmona, P. P.; Jacobs, P. A.; De Vos, D. E.; Hofkens, J.; Sels, B. F. *Angew. Chem., Int. Ed.* **2010**, *49*, 908–911.
(31) Hagfeldt, A.; Grätzel, M. *Acc. Chem. Res.* **2000**, *33*, 269–277.
(32) The possibility of a faster radiative decay, or other nonradiative decay pathways, is not ruled out. Ultrafast transient absorption measurements are strongly required to clarify the ET dynamics.
(33) Biju, V.; Micic, M.; Hu, D.; Lu, H. P. *J. Am. Chem. Soc.* **2004**, *126*, 9374–9381.
(34) Pan, D.; Hu, D.; Lu, H. P. *J. Phys. Chem. B* **2005**, *109*, 16390–16395.
(35) Pan, D.; Klymyshyn, N.; Hu, D.; Lu, H. P. *Appl. Phys. Lett.* **2006**, *88*, 093121/093121–093121/093123.
(36) Wang, Y.; Wang, X.; Ghosh, S. K.; Lu, H. P. *J. Am. Chem. Soc.* **2009**, *131*, 1479–1487.
(37) Wang, Y.; Wang, X.; Lu, H. P. *J. Am. Chem. Soc.* **2009**, *131*, 9020–9025.
(38) Guo, L.; Wang, Y.; Lu, H. P. *J. Am. Chem. Soc.* **2010**, *132*, 1999–2004.
(39) Xu, W.; Kong, J. S.; Yeh, Y.-T. E.; Chen, P. *Nat. Mater.* **2008**, *7*, 992–996.
(40) Xu, W.; Kong, J. S.; Chen, P. *J. Phys. Chem. C* **2009**, *113*, 2393–2404.
(41) Ferry, J. L.; Glaze, W. H. *J. Phys. Chem. B* **1998**, *102*, 2239–2244.
(42) Step edges at terraces are other common intrinsic defects on the surface. At the step on anatase TiO_2(101), molecular adsorption is still favored over dissociative adsorption, but the energy difference is much smaller than on the flat terrace.[43] This structural disorder may enhance the heterogeneity in the adsorptivity and reactivity.
(43) Gong, X.-Q.; Selloni, A.; Batzill, M.; Diebold, U. *Nat. Mater.* **2006**, *5*, 665–670.
(44) Wang, C.-Y.; Groenzin, H.; Shultz, M. J. *J. Am. Chem. Soc.* **2004**, *126*, 8094–8095.
(45) Tilocca, A.; Selloni, A. *J. Phys. Chem. B* **2004**, *108*, 19314–19319.

(46) Li, Y.-F.; Liu, Z.-P.; Liu, L.; Gao, W. *J. Am. Chem. Soc.* **2010**, *132*, 13008–13015.
(47) Wu, N.; Wang, J.; Tafen, D. N.; Wang, H.; Zheng, J.-G.; Lewis, J. P.; Liu, X.; Leonard, S. S.; Manivannan, A. *J. Am. Chem. Soc.* **2010**, *132*, 6679–6685.
(48) Kuznetsov, V. N.; Serpone, N. *J. Phys. Chem. C* **2007**, *111*, 15277–15288.
(49) Tachikawa, T.; Ishigaki, T.; Li, J.-G.; Fujitsuka, M.; Majima, T. *Angew. Chem., Int. Ed.* **2008**, *47*, 5348–5352.
(50) He, Y.; Dulub, O.; Cheng, H.; Selloni, A.; Diebold, U. *Phys. Rev. Lett.* **2009**, *102*, 106105/106101–106105/106104.
(51) Gong, X.-Q.; Selloni, A. *J. Phys. Chem. B* **2005**, *109*, 19560–19562.
(52) Li, S.-C.; Diebold, U. *J. Am. Chem. Soc.* **2010**, *132*, 64–66.
(53) Li, S.-C.; Chu, L.-N.; Gong, X.-Q.; Diebold, U. *Science* **2010**, *328*, 882–884.
(54) Liu, G.; Sun, C.; Yang, H. G.; Smith, S. C.; Wang, L.; Lu, G. Q.; Cheng, H.-M. *Chem. Commun.* **2010**, *46*, 755–757.